Cha et al. *Zool. Res.* 2024, 45(5): 1001−1012
https://doi.org/10.24272/j.issn.2095-8137.2023.372
https://cstr.cn/32248.14.zr.2024.372

ZR | Zoological Research

Article Open Access

Bat-derived oligopeptide LE6 inhibits the contact-kinin pathway and harbors anti-thromboinflammation and stroke potential

Li-Na Cha[1,2,#], Juan Yang[3,#], Jin-Ai Gao[2,#], Xin Lu[3], Xiao-Long Chang[3], Rebecca Caroline Thuku[1], Qi Liu[1], Qiu-Min Lu[1], Dong-Sheng Li[1], Ren Lai[1,*], Ming-Qian Fang[1,*]

[1] *Engineering Laboratory of Peptides of Chinese Academy of Sciences*, *Key Laboratory of Bioactive Peptides of Yunnan Province*, *KIZ-CUHK Joint Laboratory of Bioresources and Molecular Research in Common Diseases*, *National Resource Center for Non-Human Primates*, *National Research Facility for Phenotypic & Genetic Analysis of Model Animals (Primate Facility)*, *Key Laboratory of Genetic Evolution & Animal Models*, *Sino-African Joint Research Center*, *and New Cornerstone Science Laboratory*, *Kunming Institute of Zoology*, *Chinese Academy of Sciences*, *Kunming*, *Yunnan* 650201, *China*

[2] *School of Molecular Medicine*, *Hangzhou Institute for Advanced Study*, *University of Chinese Academy of Sciences*, *Hangzhou*, *Zhejiang* 310024, *China*

[3] *First Affiliated Hospital of Kunming Medical University*, *Kunming*, *Yunnan* 650032, *China*

ABSTRACT

Thrombosis and inflammation are primary contributors to the onset and progression of ischemic stroke. The contact-kinin pathway, initiated by plasma kallikrein (PK) and activated factor XII (FXIIa), functions bidirectionally with the coagulation and inflammation cascades, providing a novel target for therapeutic drug development in ischemic stroke. In this study, we identified a bat-derived oligopeptide from *Myotis myotis* (Borkhausen, 1797), designated LE6 (Leu-Ser-Glu-Glu-Pro-Glu, 702 Da), with considerable potential in stroke therapy due to its effects on the contact kinin pathway. Notably, LE6 demonstrated significant inhibitory effects on PK and FXIIa, with inhibition constants of 43.97 μmol/L and 6.37 μmol/L, respectively. *In vitro* analyses revealed that LE6 prolonged plasma recalcification time and activated partial thromboplastin time. In murine models, LE6 effectively inhibited carrageenan-induced mouse tail thrombosis, $FeCl_3$-induced carotid artery thrombosis, and photochemically induced intracerebral thrombosis. Furthermore, LE6 significantly decreased inflammation and stroke injury in transient middle cerebral artery occlusion models. Notably, the low toxicity, hemolytic activity, and bleeding risk of LE6, along with its synthetic simplicity, underscore its clinical applicability. In conclusion, as an inhibitor of FXIIa and PK, LE6 offers potential therapeutic benefits in stroke treatment by mitigating inflammation and preventing thrombus formation.

Keywords: PK; FXIIa; Anti-thromboinflammation; Ischemic stroke therapies; Oligopeptide

INTRODUCTION

Ischemic stroke (IS), attributable to a cascade of events such as hypoxia (Li et al., 2022; Pei et al., 2020), inflammation, oxidative stress, and neuronal cell death due to sudden arterial blockage by thrombosis, accounted for 62.4% of all new strokes in 2019, making it the leading cause of disability and death globally (Chamorro et al., 2016; GBD 2019 Stroke Collaborators, 2021). Plasma kallikrein (PK), encoded by the *KLKB1* gene, plays a pivotal role in various physiological and pathological processes, including blood coagulation, inflammatory response, vascular function regulation, and IS development and progression. PK traditionally cleaves high-molecular-weight kininogen (HK) to release bradykinin (BK), a pro-inflammatory hormone, and interacts with factor XII (FXII) (active form FXIIa) to autoactivate the contact-kinin system

Received: 29 February 2024; Accepted: 30 April 2024; Online: 01 May 2024
Foundation items: This work was supported by the National Natural Science Foundation of China (32200397, 23SWAQ09, and 31930015), Yunnan Province Grant (202302AA310032, 202302AA310035, and 202003AD150008), Ministry of Science and Technology of China (2018YFA0801403), Chinese Academy of Sciences (SAJC202103 and KFJ-BRP-008-003), New Cornerstone Investigator Program (NCI202238), Kunming Science and Technology Bureau (2022SCP007), Priority Union Foundation of Yunnan Provincial Science and Technology Department and Kunming Medical University (202101AC070461), and Basic Research Program of Yunnan Province Science and Technology Department (202301AT070083)

[#]Authors contributed equally to this work

*Corresponding authors, E-mail: rlai@mail.kiz.ac.cn; fangmingqian@mail.kiz.ac.cn

and promote thrombus formation via the intrinsic pathway (Zamolodchikov et al., 2015, 2016). This interaction underscores the link between thrombosis and inflammation (Göb et al., 2015; Göbel et al., 2019; Kearney et al., 2021; Kleinschnitz et al., 2006; Renné et al., 2005; Sala-Cunill et al., 2015).

Animal models have significantly advanced our understanding of thromboinflammation pathophysiology. Research involving kallikrein deficient mice (*Klkb1*$^{-/-}$), FXII-deficient mice (*F12*$^{-/-}$), and inhibitor-treated mice has demonstrated prolonged activated partial thromboplastin time (APTT) (Aygören-Pürsün et al., 2016; Ivanov et al., 2020; Kale et al., 2018; Renné, 2005). Furthermore, *Klkb1*$^{-/-}$ mice exhibit increased resistance to $FeCl_3$-induced carotid artery thrombosis, while *F12*$^{-/-}$ mice and those with selective PK reduction via antisense oligonucleotides show reduced thrombus formation without bleeding abnormalities (Bird et al., 2012; Revenko et al., 2011; Simão et al., 2017). In collagen/epinephrine-induced pulmonary embolism models, *Klkb1*$^{-/-}$ mice display reduced lung perfusion and inflammation due to decreased BK formation, yet maintain normal vessel fibrin formation and platelet activation following acute lung injury, indicating preserved hemostasis (Renné, 2015). Additionally, most PK- and FXIIa-deficient patients do not exhibit hemostatic defects (Girolami et al., 2011; Kearney et al., 2021; Kenne & Renné, 2014; Sala-Cunill et al., 2015). Thus, inhibition of PK and FXIIa may represent a promising therapeutic strategy for thromboembolic conditions by suppressing thromboinflammation while preserving hemostasis. Blockade of PK or FXIIa has been shown to ameliorate stroke injury in middle cerebral artery occlusion (MCAO) mouse models by reducing thromboinflammation, without increasing bleeding risk (Frazier et al., 2023; Göb et al., 2015; Kleinschnitz et al., 2006; Simão et al., 2017). Although PK and FXIIa inhibitors are not yet widely applied in clinical stroke therapy, their potential as safer and more effective stroke treatments is gaining considerable attention.

Anti-thromboinflammatory peptides, such as ecallantide (Zuraw et al., 2010), sylvestin (Zhang et al., 2022), NP1 (Li et al., 2023b), and OM-LV20 (Yin et al., 2022), are noted for their safety and efficacy in stroke therapy. However, their commercialization has been hindered by the high costs associated with their long peptide sequences and the need to maintain their secondary structures. In the current study, we identified a six-amino-acid oligopeptide, Leu-Ser-Glu-Glu-Pro-Glu (LSEEPE, LE6), derived from *Myotis myotis* (Borkhausen, 1797), which interacts with the active sites of PK and FXIIa to exert inhibitory effects. Notably, LE6 demonstrated profound protection against IS in mice by attenuating thromboinflammation without substantially prolonging bleeding time. Thus, LE6 demonstrates potential therapeutic benefits in stroke treatment by inhibiting FXIIa and PK, thereby reducing inflammation and preventing thrombus formation, making it a promising candidate for further research and clinical development.

MATERIALS AND METHODS

Animals and ethics statement

Male C57BL/6J and BALB/c mice (6 weeks old) were purchased from Beijing Charles River Laboratories (China) and housed in a pathogen-free environment. The mice were provided with high-pressure-treated food and water and maintained under a 12/12-h light/dark cycle at 24°C. The bat brain homogenates were kindly provided by Dr. Qi Liu from the State Key Laboratory of Genetic Resources and Evolution, Kunming Institute of Zoology (China). All animal experiments were conducted with the approval of the Ethics Committee for Laboratory Animal Welfare of the Kunming Institute of Zoology, Chinese Academy of Sciences (approval number: IACUC-RE-2023-05-015).

Co-immunoprecipitation (Co-IP) and liquid chromatography-tandem mass spectrometry (LC-MS) analysis

Potential molecules interacting with PK in the bat brain were identified using Co-IP and LC-MS. Initially, 600 μL of bat brain homogenate (5 mg/mL in 25 mmol/L Tris-HCl buffer, pH 7.4) was mixed with 50 μL of human plasma, 30 μL of Dynabeads™ Protein A (10002D, ThermoFisher Scientific, USA), and 5 μL of anti-PK 1B (KLKB1) antibody (ab44392, Abcam, UK) or control immunoglobulin G (IgG, 5 μg, NI01, Sigma, USA), then incubated at 25°C for 1 h. A centrifuge tube (1.5 mL) containing the reaction solution was placed on a magnetic separator stand (HY-K0200, MedChemExpress, USA) and washed four times with 1 mL of Tris-HCl buffer. Subsequently, 100 μL of 1×loading buffer (CW0027A, CWBIO, China) was added, and the solution was boiled for 5 min to obtain the coupled proteins. All proteins were subjected to 12% sodium dodecyl sulfate-polyacrylamide gel electrophoresis (SDS-PAGE). The protein lanes were excised and sent to Novogene (China) for gel digestion and LC-MS analysis using a Q Exactive™ Hybrid Quadrupole-Orbitrap™ Mass Spectrometer (ThermoFisher Scientific, USA).

Molecular docking

AutoDock v.4.2 was used for molecular docking. During the docking process, the KLKB1 protein (PDB code:6O1S) was maintained in a rigid state while the LE6 peptide was maintained in a flexible state. The grid box dimensions were set to 60 Å×60 Å×60 Å. The grid center was positioned proximate to the three active residues of KLKB1 (His428, Asp483, and Ser578). The grid spacing was defined at 0.375 Å. In total, 250 Lamarckian Genetic Algorithm (LGA) runs were performed, yielding 270 000 generations, and the energy evaluation value was set to 25 000 000. All other parameters were set to default. Subsequently, the process yielded 250 conformations, which were subjected to cluster analysis according to their root mean square deviation (RMSD). The conformation in the largest cluster with the lowest energy was regarded as the optimal docking conformation.

Cytotoxicity assay

Human embryonic kidney 293T cells (HEK 293T cells) were purchased from the Kunming Cell Bank of the Chinese Academy of Sciences (China). The HEK 293T cells were cultured in Dulbecco's Modified Eagle Medium/Nutrient Mixture F-12 (DMEM/F-12, 10-092-CVR, Corning, USA) containing 10% fetal bovine serum (FBS, 35-081-CV, Corning, USA) and 1% penicillin-streptomycin solution (P1400, Solarbio, USA).

Mouse peritoneal macrophages and splenocytes were collected, as described previously (Fang et al., 2023a). Macrophages were collected from mice by daily intraperitoneal injections of 3% sterile Fluid Thioglycollate Broth (42634, Biomerieux, France) to stimulate macrophage proliferation,

and cultured macrophages were collected by PBS lavage of the peritoneal cavity after 3 days. And splenocytes were obtained from freshly harvested mouse spleens by crushing in PBS and passing through a 200-mesh sieve. Both cells were cultured in RPMI1640 complete medium (10-040-CVR, Corning, USA). All cells were grown at 37°C with 5% CO_2.Analysis of the effects of LE6 on the viability of HEK 293T cells, mouse primary splenocytes, and mouse peritoneal macrophages was performed using a cell counting kit-8 (CCK8) (GK10001, GLPBIO, USA). The HEK 293T cells (3×10^4 cells/well), mouse peritoneal macrophages (1×10^6 cells/well), and mouse primary splenocytes (2×10^5 cells/well) were seeded in 96-well plates (Thermo, 167008, USA). After 12 h cultivation for adherence, the cells were treated with varying concentrations of LE6 (200, 100, 50, 25, 12.5, 0 μg/mL) for 8 h, followed by the addition of 10 μL of CCK-8 reagent to each well and further incubation for 3 h. An enzyme-labeled instrument (Epoch BioTek, USA) was used to detect chromogenic data at $OD_{450\ nm}$. Cell viability was expressed as a percentage relative to the control group.

Hemolysis assay

To explore the effects of LE6 on hemolysis, blood samples were obtained from the First Affiliated Hospital of Kunming Medical University (approval ID: KIZZRKX-2023-05) and immediately centrifuged for 10 min at 3 500 r/min and 25°C. After removing the supernatant, the obtained erythrocytes were resuspended in phosphate-buffered saline (PBS, 0.01 mol/L, pH 7.2) and incubated with the positive control Triton-X100 (0.1%) and different concentrations of LE6 (98% purity, chemically synthesized by GL Biochem (China)) (200, 100, 50, 25, 12.5, 0 μg/mL) for 30 min at 37 °C, followed by centrifugation at 3 500 r/min and 37°C for 5 min. The resulting supernatant was subjected to absorbance detection at 540 nm using the enzyme-labeled instrument.

Bleeding assay

Bleeding times were determined according to previously published procedures (Holland, 1976). LE6 (0.5 and 2 mg/kg), 0.9% saline, and heparin sodium (2 500 U/kg, 9041-08-1, BIOFROX, Germany) were first injected intravenously (*i.v.*) (15 min before operation) into male C57BL/6 J mice (6 weeks old, 18–20 g, *n*=6–7). Their tails were then cut 2 mm from the tip and carefully immersed in sterile saline at 37°C. Bleeding time was recorded until the blood flow ceased.

Plasma recalcification time (PRT)

For PRT testing *in vitro*, 20 μL of human plasma was incubated with different concentrations of LE6 (500, 250, 125, 62.5, 0 μmol/L) in 60 μL of HEPES buffer (25 mmol/L 4-(2-hydroxyethyl)-1-piperazineethanesulfonic acid (HEPES), 150 mmol/L NaCl, pH 7.4) for 5 min at 37°C, followed by the addition of 60 μL of HEPES buffer with 25 mmol/L $CaCl_2$. Clotting was monitored at 650 nm.

For PRT testing *in vivo*, 30 μL of mouse plasma (mixing blood and 3.8% sodium citrate in a 3:1 volume ratio) obtained 15 min after *i.v.* injection of heparin sodium, 0.5 or 2 mg/kg LE6 was incubated with 60 μL of HEPES buffer at 37°C for 5 min. Kinetic analyses were conducted immediately after the addition of Ca^{2+} (60 μL of HEPES buffer with 25 mmol/L $CaCl_2$) using a zymography instrument. Clotting time was calculated by measuring the time to a half-maximal increase in OD_{650nm}.

APTT and prothrombin time (PT)

APTT (GMS10178.2, Genmed, USA) and PT (STY50101, Steellex, China) assays were performed using commercial kits following the manufacturer's instructions. Kinetic monitoring of absorption values was conducted at 650 nm with an enzyme-labeled instrument (Epoch 109 BioTek, USA).

Chromogenic assay

The effects of LE6 on coagulation and fibrinolytic system enzymes, such as PK (HPKa1303, Enzyme Research, USA), FXIIa (HFXIIa1212a, Enzyme Research, USA), tissue plasminogen activator (tPA) (HY-P71051, MedChemExpress, USA), urokinase plasminogen activator (uPA) (HY-P71050, MedChemExpress, USA), and plasmin (HPlasmin, Enzyme Research, USA) were detected using different corresponding chromogenic substrates. In brief, 110 nmol/L PK, 0.63 nmol/L FXIIa, 0.72 nmol/L tPA, 2.36 nmol/L uPA, and 1.6 nmol/L plasmin were incubated with LE6 at different concentrations (0–285 μmol/L) at 37°C for 5 min in 50 μL of PBS, followed by the addition of 50 μL of H-D-prolyl-L-phenylalanyl-L-arginine-p-nitroaniline dihydrochloride (Chromogenix S-2302™, Diapharma, USA) for PK (408 and 816 μmol/L) and FXIIa (216 and 433 μmol/L) chromogenic reactions, and 433 μmol/L H-D-isoleucyl-L-prolyl-L-arginine-p-nitroaniline dihydrochloride (Chromogenix S-2288TM, Diapharma, USA) for tPA, uPA, and plasmin chromogenic reactions. Absorbance was immediately monitored at 405 nm for 30 min. Dixon plot curves were used to calculate the inhibition constant (*K*i) of LE6 for PK and FXIIa.

Surface plasmon resonance (SPR) analysis

SPR analysis was performed following the manufacturer's instructions. A series S sensor chip CM5 (10306700, Cytiva, USA) was first equilibrated with PBS at a flow rate of 5 μL/min for 2 min. The target channel was then activated using a solution of 0.4 mol/L 1-ethyl-3-(3-dimethylaminopropyl) carbodiimide hydrochloride mixed with 10 mmol/L N-hydroxysuccinimide at a flow rate of 5 μL/min for 20 min, with 200 μL of sodium acetate (10 mmol/L, pH 4.0, 18-1068, Sartorius, Germany) containing 500 μg/mL LE6 passed over the surface of the activated channel to achieve a response value of 2 000 response units (RUs). Thereafter, ethanolamine (1 mol/L, pH 8.5, 18-1071, Sartorius, Germany) was used to block the chip channel at a flow rate of 5 μL/min for 15 min. Real-time detection was performed using a Biacore T200 instrument (General Electric Company, USA) at a flow rate of 5 μL/min. To assess the binding interactions between LE6 and various enzymes, different concentrations of PK (0–210 nmol/L in PBS), FXIIa (0–200 nmol/L in PBS), tPA (0-200 nmol/L in PBS), uPA (0–200 nmol/L in PBS), and plasmin (0–1 000 nmol/L in PBS) were flowed over the LE6-coupled chip at a flow rate of 20 μL/min. The association rate constant (*K*a), dissociation rate constant (*K*d), and equilibrium dissociation constant (*K*D) were subsequently determined using the BIA evaluation program.

Thrombosis models

For $FeCl_3$-induced carotid artery thrombosis, male C57BL/6J mice (6 weeks old) were anesthetized after an *i.v.* injection of 100 μL of 0.9% saline (control), 2 500 U/kg heparin sodium, 0.5 or 2 mg/kg LE6 following previously described procedures (Tang et al., 2020). The left carotid artery was carefully separated, and a circular pad with a 2 mm radius was positioned beneath the artery to minimize background blood flow disturbances. Subsequently, a filter paper soaked with

10% $FeCl_3$ (w/v) solution was applied to the artery for 30 s of contact, then removed. Changes in the region of interest (ROI) were monitored and recorded using a real-time laser speckle (RWD, China) perfusion (LSP) imaging system and SIM BFI software (SIM BFI HR Pro, Simopto, China). Thrombus occlusion was considered to have occurred when the vessel in the images changed from red to blue. The duration for continuous recording was set to 30 min. Mice in which the time from the start of surgery to $FeCl_3$ induction exceeded 5 min, or those exhibiting severe surgical hemorrhage, were excluded from data analysis.

For carrageenan-induced tail thrombosis, male BALB/c mice (6 weeks old) were *i.v.* injected with saline (control), heparin sodium (2 500 U/kg), or LE6 (0.5 and 2 mg/kg), then intraperitoneally (*i.p.*) injected with 200 μL of 1% carrageenan (type I) (CC3171, Coolaber, China) dissolved in 0.9% saline. After 24 h, tail thrombus length was observed and recorded.

Cortical photothrombosis stroke (CPS) model

Male C57BL/6J mice (6 weeks old, *n*=6–7) were *i.p.* injected with 50 mg/kg Rose Bengal 1 h prior to surgery, then *i.v.* injected with 0.9% saline (control), heparin sodium (2 500 U/kg), or LE6 (0.5 or 2 mg/kg) 5 min prior to surgery. Mice were anesthetized and an incision was created along the midline from the level of the eye down to the neck to expose the skull, following previously reported methods (Labat-Gest et al., 2013). The target area was irradiated for 7 min using a 562 nm yellow-green light laser (R-LG561-100-A5, RWD, China) at 15 mW. Mice underwent LSP imaging 1 day post-CPS surgery. Mouse survival was recorded over 15 consecutive days of administration.

60 min Transient middle cerebral artery occlusion (tMCAO) model

Male C57BL/6J mice (6 weeks old, *n*=6–7) were first anesthetized and fixed on a thermo-controlled operating table (Harvard Apparatus, USA) to maintain a normal body temperature (37°C) during tMCAO surgery. A wire bolus (1623-50A4, CNONTECH, China) was inserted from the external carotid artery (ECA) into the internal carotid artery (ICA) following previously reported protocols (Fang et al., 2023a). Saline (0.9%) or LE6 (0.5 or 2 mg/kg) was intravenously (i.v.) injected 15 min before the wire was removed. After 60 min of occlusion, the wire was removed to allow reperfusion. Mice that died within 24 h post-tMCAO or had operation times exceeding 15 min were excluded from endpoint analysis.

To assess neurological function and infarct size 24 h post-tMCAO, mice were subjected to Bederson and grip scoring, then sacrificed for 2% 2,3,5-triphenyl tetrazolium chloride (TTC) staining. To assess intracerebral blood-brain barrier (BBB) function and inflammation, a subset of mice received an *i.v.* injection of 200 μL of 0.5% Evans blue staining solution (R20616, Yuanye Bio-Technology, China) immediately after tMCAO surgery, with brain sections imaged 24 h later. Additionally, brain homogenates and serum samples were collected from another group of mice 24 h post-surgery for analysis of lipopolysaccharide-binding protein (LBP) (DG95654Q, Dogesce, China), interleukin-1β (IL-1β) (DG30045M, Dogesce, China), tumor necrosis factor alpha (TNF-α) (DG30048M, Dogesce, China), and C-X-C motif chemokine ligand 1 (CXCL1) (DG91491Q, Dogesce, China) levels using commercial enzyme-linked immunosorbent assay (ELISA) kits following the manufacturer's instructions.

Bederson scores and grip strength test (GST)

The Bederson neurological function scoring criteria were as follows: 0, no behavioral disorders; 1, inability to extend the right forelimb; 2, rotation to the right; 3, tilting to the right; 4, no voluntary activities accompanied by disturbance of consciousness; and 5, death. For the GST, mouse grip strength was measured using a Grip Strength Meter (DS2-50N, Sansbio, China) in accordance with the manufacturer's instructions.

TTC staining

Infarct volume was evaluated using TTC staining (T-8877, Sigma-Aldrich, USA). Mice were sacrificed, and their intact brains were carefully removed and immediately placed in a mouse brain sectioning mold (Harvard Apparatus, USA) for cutting to 2 mm thick coronal sections. Subsequently, the sections were stained with 2.0% TTC at 37°C for 20 min and imaged. Brain infarct volume was measured volumetrically with ImageJ software (NIH, USA) using the equation: $V=Sd/T^2$, where S is the infarct area, d is the thickness, and T is the linear magnification.

Statistical analysis

TTC-stained and Evans blue-stained images were quantified using ImageJ v.1.52a and Image Pro Plus v.6.0. Analyses were performed using GraphPad Prism v.6.0 and SPSS v.20. Data are presented as mean±standard error of the mean (SEM). One-way analysis of variance (ANOVA) followed by Fisher's protected *t*-test were performed, with $P \leq 0.05$ considered significant. At least two independent replicates of each experiment were performed.

RESULTS

Bat-derived oligopeptide LE6 directly inhibits PK and FXIIa

Considering the important role of PK in the contact-kinin pathway (Göb et al., 2015; Göbel et al., 2019; Kearney et al., 2021), we performed Co-IP analysis using an anti-PK antibody to pulldown potential molecules interacting with PK in the brain of *Myotis myotis*. Peptides and proteins from the bat brain that bound to PK were identified by LC-MS analysis. The optimal inhibitory activity and shortest fragment sequence for PK inhibition, Leu-Ser-Glu-Glu-Pro-Glu (LSEEPE, LE6), was characterized through molecular docking and enzymatic kinetic activity screening, revealing that LE6 predominantly bound to the reactive loop in the protease domain of PK (Figure 1A). Thus, LE6 (98% purity) was chemically synthesized for subsequent biological functional analysis.

SPR measures the binding capacity, affinity, and kinetics between biomolecules. As depicted in Figure 1B, RUs increased with reaction from 0 to 60 s, indicating binding interaction between LE6 and PK. The increase in RUs was more pronounced at higher concentrations of LE6, with the highest concentration (210 nmol/L) reaching an RU value of 100, demonstrating high binding affinity. The *K*a, *K*d, and *K*D values for the LE6-PK interaction were 1.79×10^3 mol/L/s, 1.41×10^{-2} per s, and 7.88 μmol/L, respectively. To further investigate the impact of LE6 on PK activity, enzyme kinetic assays using specific chromogenic substrates were performed. As shown in Figure 1C, LE6 exhibited a dose-dependent inhibition of PK activity, reducing its ability to degrade the chromogenic substrate across a concentration gradient of 0–285 μmol/L. The half-maximal inhibitory

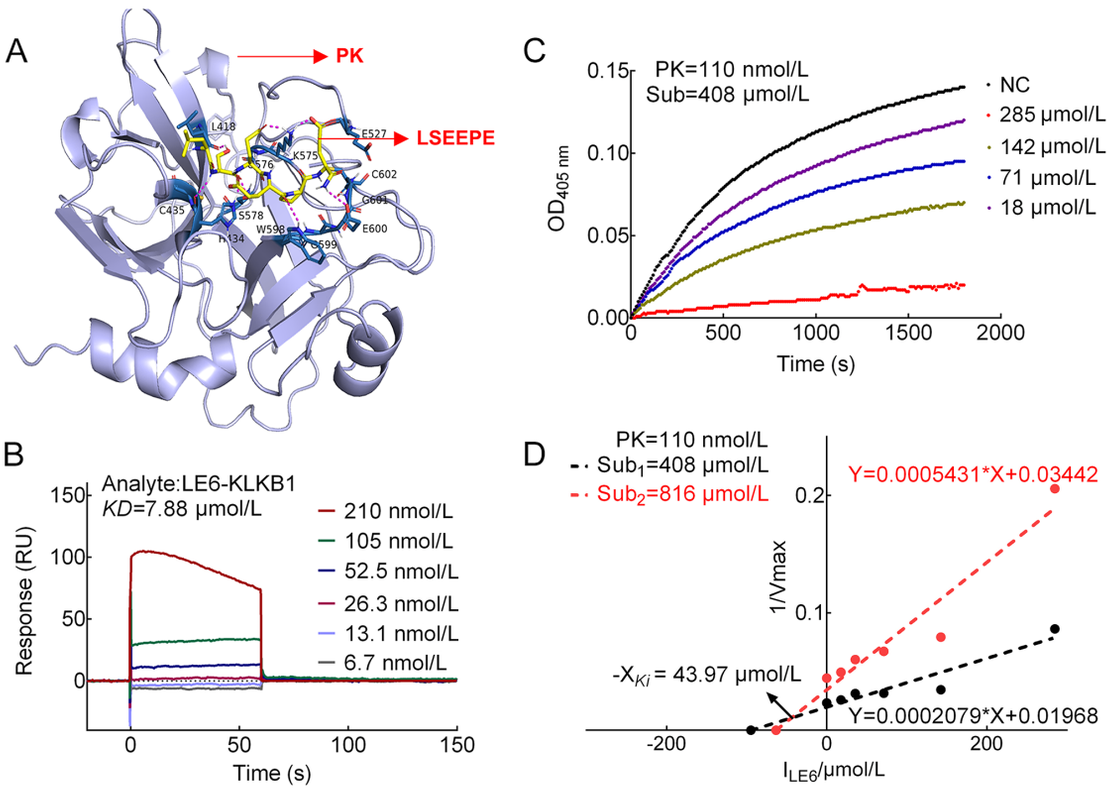

Figure 1 Oligopeptide LE6 inhibits PK activity

A: 3D structure illustrating optimal docking conformation of LE6 and PK using AutoDock v.4.2. B: SPR analysis of interaction between LE6 (6.7–210 nmol/L) and PK. C: Enzyme kinetic analysis of effects of LE6 (0–285 μmol/L) on PK activity. D: Dixon plot illustrating *K*i (43.97 μmol/L) of LE6 on PK. PK, KLKB1: Plasma kallikrein; *K*i: Inhibition constant; *K*D: Equilibrium dissociation constant.

concentration (IC_{50}) was approximately 71 μmol/L. Additionally, the *K*i value for LE6 on PK was 43.97 μmol/L, as shown in the Dixon plot (Figure 1D). Collectively, these results indicate that LE6 effectively inhibits PK activity.

The contact-kinin pathway, involving PK and FXIIa, triggers a cascade of reactions in the coagulation process, leading to the sequential activation of FXI, FIX, FVIII, FX, FII, and FXIII, ultimately culminating in fibrous clot formation (Göb et al., 2015; Göbel et al., 2019; Kearney et al., 2021). Here, SPR analysis demonstrated a strong interaction between LE6 and FXIIa, with *K*a, *K*d, and *K*D values of 2.25×10^3 mol/L/s, 1.18×10^{-1} per s, and 46.4 μmol/L, respectively (Figure 2A). Further analysis of the effects of LE6 on FXIIa activity using chromogenic substrates revealed dose-dependent inhibition. As shown in Figure 2B, C, LE6 significantly inhibited FXIIa activity, achieving an inhibition rate of 88.59%±1.74% (mean±SEM) at the highest concentration of 285 μmol/L, compared to the PBS-treated group (negative control, NC). Notably, significant inhibition was observed even at the lowest concentration of 9 μmol/L (*P*=0.0368). The IC_{50} of LE6 on FXIIa was 71 μmol/L, equivalent to the inhibitory effect of PK. Dixon plot analysis determined the *K*i of LE6 against FXIIa to be 6.37 μmol/L (Figure 2D), indicating a stronger inhibitory potential on FXIIa compared to PK. Among the enzymes of the coagulation system, LE6 primarily targeted PK and FXIIa and their mutual activation, thereby inhibiting the contact-kinin pathway to suppress both inflammation and thrombosis.

LE6 is a low-cytotoxic oligopeptide that prevents thrombosis with low risk of bleeding

Before conducting a detailed functional study of the bioactivity of LE6, a preliminary assessment of its safety was performed using hemolytic activity and cell viability assays. Results showed that LE6 exhibited no hemolytic side effects *in vitro*, even at a high concentration of 200 μg/mL (285 μmol/L) (Figure 3A). Furthermore, cell viability assays using CCK8 demonstrated that LE6 had no toxic effects on the proliferation of HEK 293T cells (Figure 3B), mouse splenocytes (Figure 3C), and mouse peritoneal macrophages (Figure 3D) at concentrations ranging from 12.5 to 200 μg/mL.

The contact-kinin pathway contributes to thrombus formation within the endogenous coagulation pathway and operates independently from the exogenous coagulation pathway (Long et al., 2016). We hypothesized that LE6 may inhibit thrombus formation without inducing hemorrhage by inhibiting FXIIa and PK. To confirm this speculation, RPT (Figure 4A), APTT (Figure 4B), and PT (Figure 4C) analyses were performed *in vitro*. Results showed that LE6 significantly and dose-dependently prolonged PRT and APTT at concentrations of 125, 250, and 500 μmol/L, while a significant prolongation of PT was observed only at the highest concentration of 500 μmol/L. APTT and PT are indicative of the coagulation capacities of the endogenous and exogenous coagulation pathways, respectively. Thus, high concentrations of LE6 may inhibit both pathways, suggesting the presence of an unknown target associated with bleeding risk at higher doses. Indeed, the inhibitory effect of LE6 on high bleeding risk activators such as tPA (Figure 4D, E), uPA (Figure 4F, G), and plasmin (Figure 4H, I) provides a rationale for the possible reduction of bleeding in future clinical applications.

Animal experiments provided further validation of our hypothesis. As demonstrated in Figure 4J, K, *i.v.* injection of 0.5 mg/kg LE6 significantly prolonged PRT without notably extending bleeding time of severed tail tips in mice. Although

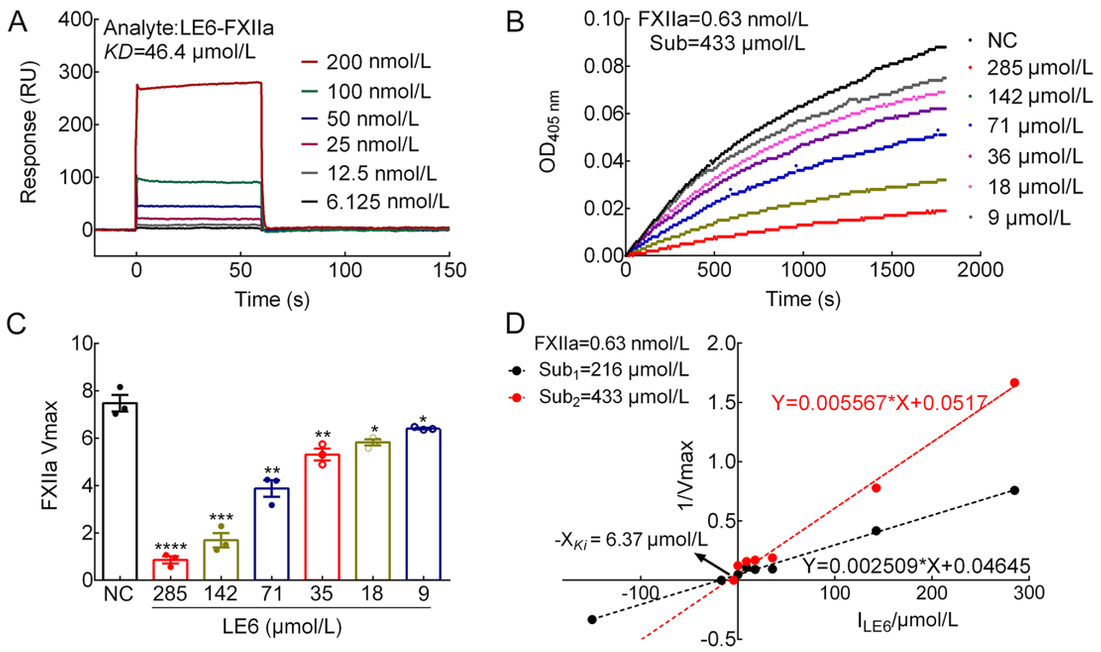

Figure 2 LE6 interacts with and inhibits FXIIa activity

A: SPR analysis of interaction between LE6 (6.125–200 nmol/L) and FXIIa. B, C: Enzyme kinetic analysis of effects of LE6 (0–285 μmol/L) on FXIIa activity, with maximum velocity (Vmax) measurements from (B) recorded in (C) (n=3). D: Dixon plot illustrating Ki (6.37 μmol/L) of LE6 on FXIIa. One-way ANOVA with Fisher's protected t-test was used in panel C. *: P<0.05; **: P<0.01; ***: P<0.001; ****: P<0.0001. Data are presented as mean±SEM. FXIIa: Activated factor XII; NC: Negative control.

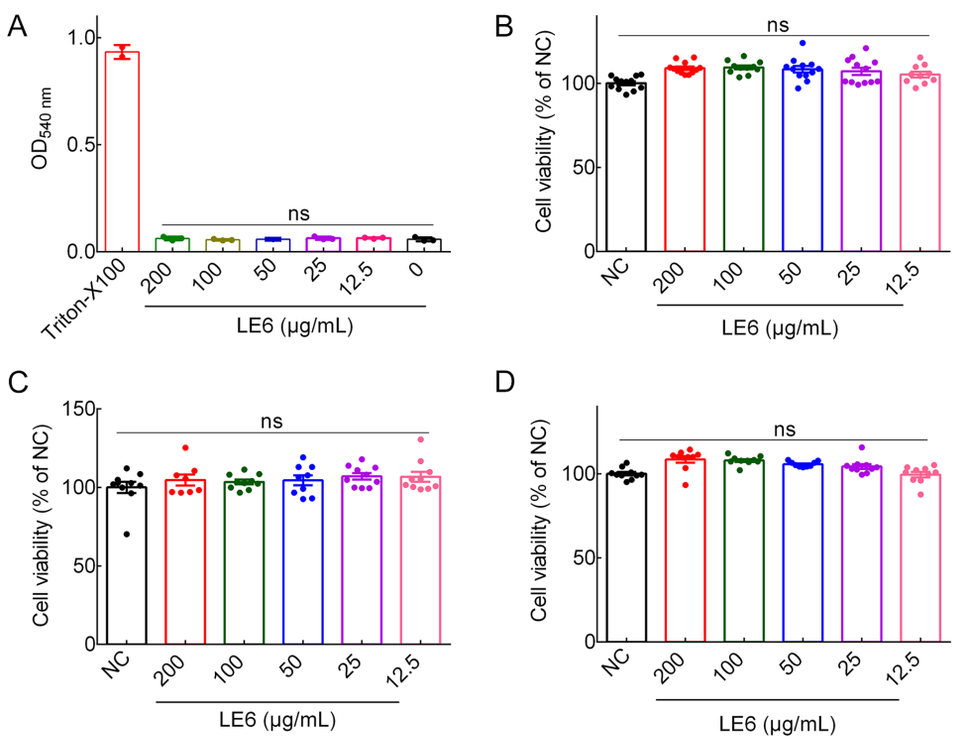

Figure 3 LE6 exhibits no hemolytic activity or cytotoxicity

A: Hemolysis of hemocytes after treatment with 0.1% Triton-X 100 (positive control) or different concentrations of LE6 (0–200 μg/mL) (n=2–3). B–D: Percentage of viable HEK 293T cells (B), mouse splenocytes (C), and mouse peritoneal macrophages (D) after 24 h of incubation with 0–200 μg/mL LE6, as quantified by CCK8 assay (n=8–12). One-way ANOVA with Fisher's protected t-test was performed for data analysis. ns: Not significant. Data are presented as mean±SEM. CCK8: Cell counting kit-8.

LE6 significantly prolonged bleeding time at a higher dose of 2 mg/kg, bleeding time was approximately half that induced by the clinically anticoagulant heparin sodium (2 500 U/kg, *i.v.*), indicating that LE6 generally presents a lower risk of bleeding.

To investigate the effect of LE6 on thrombosis, carrageenan-induced tail and $FeCl_3$-induced carotid arterial thrombosis mouse models were used. Carrageenan, a potent proinflammatory agent, triggers local thrombosis in the tail

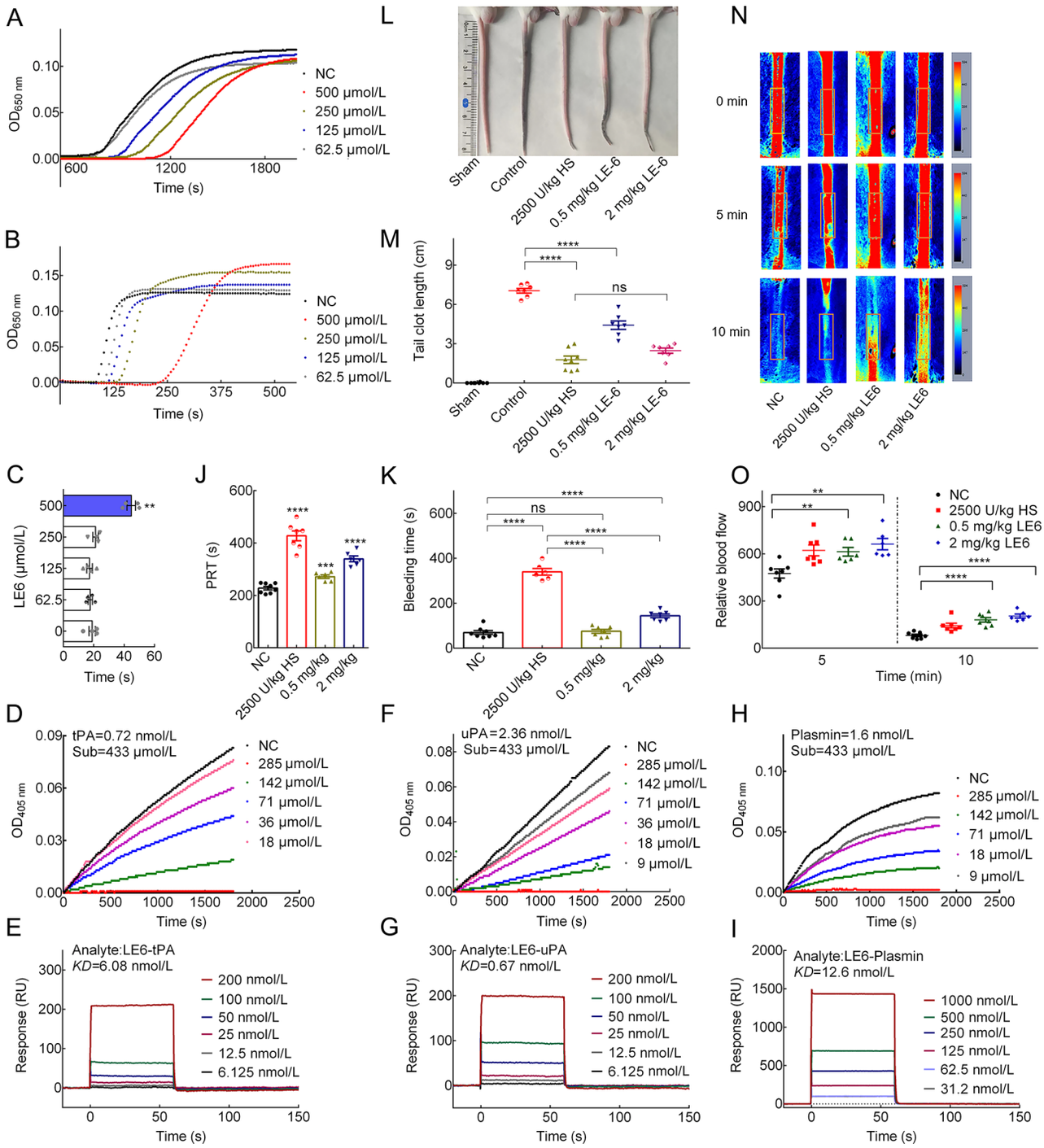

Figure 4 LE6 inhibits coagulation and thrombosis with low bleeding risk

A–C: Effects of LE6 (0–500 μmol/L) on coagulation function *in vitro*, including PRT (A), APTT (B), and PT (C). D–I: SPR and enzyme kinetic analysis of interactions between LE6 and tPA (D, E), uPA (F, G), and plasmin (H, I). J, K: Male C57BL/6J mice (6 weeks old) were *i.v.* injected with 0.9% saline (control), heparin sodium (2 500 U/kg), or LE6 (0.5 or 2 mg/kg). Bleeding time was recorded (J), and plasma was collected for PRT analysis immediately after sacrifice (K). n=6–7. L, M: Effects of LE6 on carrageenan-induced mouse tail thrombosis. Male C57BL/6J mice (6 weeks old) were photographed (L) and measured (M) for length of tail thrombus accumulation 24 h after carrageenan and drug treatment. n=6–7. N, O: Effects of LE6 on $FeCl_3$-induced arterial thrombosis. Male C57BL/6J mice (6 weeks old) were *i.v.* injected with 0.9% saline (control), heparin sodium (positive drug, 2 500 U/kg), or LE6 (0.5 or 2 mg/kg) 5 min before $FeCl_3$ induction. Blood perfusion in the carotid artery ROI (boxed area) was monitored by LSP imaging 30 s after $FeCl_3$ induction. Intravascular blood flow was imaged at 5 min and 10 min (N) and ROI values were analyzed (O). Color bar indicates perfusion unit scale (0–600). n=6–7. One-way ANOVA with Fisher's protected t-test was used in panels C, J, K, M, and O. **: P<0.01; ****: P<0.0001; ns: Not significant. Data are presented as mean±SEM. PRT: Plasma recalcification time; APTT: Activated partial thromboplastin time; PT: Prothrombin time; tPA: Tissue plasminogen activator; uPA: Urokinase plasminogen activator; LSP: Laser speckle perfusion; ROI: Region of interest.

veins of animals, making carrageenan-induced tail models suitable for assessing the efficacy of anti-inflammatory thrombotic drugs (Frazier et al., 2023; Wei et al., 2022). As a contact-kinin system inhibitor, LE6 reduced the length of carrageenan-induced mouse tail thrombi in a dose-dependent manner, achieving comparable inhibitory efficacy to the control group (P=0.0726) (Figure 4L, M). In the $FeCl_3$-induced carotid arterial thrombosis model, the application of 10% $FeCl_3$ causes localized endothelial damage, thereby activating the endogenous coagulation system and inducing complex thrombosis (Frazier et al., 2023; Revenko et al., 2011). Real-time blood flow monitoring (Figure 4N) and quantitative analysis of blood flow in the main vascular sites affected by $FeCl_3$ (boxed) (Figure 4O) showed that, compared to the PBS-treated group, *i.v.* injection of 2 500 U/kg heparin sodium, 0.5 mg/kg LE6, and 2 mg/kg LE6 increased blood flow at 5 min and 10 min post $FeCl_3$-induction. These findings suggest that LE6 exerts a notable thrombotic inhibitory effect with a low risk of bleeding.

LE6 elevates survival in the CPS model

To assess the therapeutic potential of LE6 in thrombotic stroke, a model of focal cerebral ischemia induced by photothrombosis of cortical microvessels was utilized. Thrombotic cerebral infarction was induced through an *i.p.* injection of Rose Bengal, a photosensitive dye, followed by focused illumination through the skull (Lee et al., 2007). Results showed that administration of LE6 (0.5 and 2 mg/kg, *i.v.*) significantly reduced thrombotic clot formation and increased cortical blood flow in the brains of mice on day 2 post-CPS surgery compared to the control group (Figure 5A, B). Survival rates were monitored over a 15-day period following surgery. Mice in the control group exhibited signs of distress, including dull coat, reduced appetite, weight loss, lethargy, and hunched posture, with only a 50% survival rate by day 15 (Figure 5C). In contrast, mice treated with 0.5 and 2 mg/kg LE6 displayed better overall condition, with survival rates of 67% and 73% by day 15, respectively (Figure 5C). These findings suggest that LE6 may enhance survival rates in mice following IS by preventing thrombus formation.

LE6 alleviates neurobehavioral and cerebral tissue destruction in tMCAO mice

Ischemia resulting from thrombus blockage in the cerebral blood vessels can lead to stroke injury. The tMCAO model effectively mimics the cerebral vascular blockage and revascularization typically observed in stroke patients, enabling the exploration of cerebral ischemia-reperfusion injury mechanisms and evaluation of potential therapeutic strategies by assessing neurobehavioral function, cerebral histopathological processes, and inflammatory responses (Nitzsche et al., 2021; Shuaib et al., 2011; Yan et al., 2020b). As shown in Figure 6A, B, *i.v.* administration of varying concentrations of LE6 15 min prior to reperfusion markedly improved cerebral neurological function 24 h after tMCAO surgery. This improvement was evidenced by lower Bederson scores (Figure 6A) and higher grip strength (Figure 6B) compared to the control group. Moreover, ischemia-reperfusion-induced brain tissue damage was markedly attenuated by *i.v.* injection of LE6 at both 0.5 and 2 mg/kg doses, as illustrated in the imaging (Figure 6C) and quantification (Figure 6D) of TTC staining, where viable cells were stained red and damaged areas appeared white.

LE6 reduces intracerebral inflammation and protects the BBB in tMCAO mice

Ischemia and reperfusion contribute to BBB disruption, leading to inflammatory responses, neuronal damage, and cerebral edema as blood components infiltrate brain tissue (Franke et al., 2021; Gao et al., 2021). To evaluate BBB integrity, Evans blue dye was *i.v.* injected into mice, with the extent of staining indicating the degree of BBB damage. Analysis revealed that 24 h post-tMCAO operation, the brain sections of control mice exhibited a stained area of 25.23%±1.57% (mean±SEM), while *i.v.* administration of 0.5 and 2 mg/kg LE6 reduced the stained area to 15.45%±1.04% and 9.25%±0.77%, respectively, revealing BBB-protective effects (Figure 7A, B). The contact-kinin pathway plays a central role in the thrombotic inflammatory pathology of IS (Wei et al., 2022). The anti-inflammatory effects of LE6 on IS injury were further assessed. Results showed that LE6 dose-dependently decreased the serum and brain levels of the inflammation-related mediator LBP (Figure 7C), proinflammatory factors IL-1β (Figure 7D) and TNF-α (Figure 7E), and chemokine CXCL1 (Figure 7F) in tMCAO mice.

Collectively, these findings support the potential of the contact-kinin pathway inhibitor LE6 as a therapeutic agent for inflammatory thrombosis and IS (Figure 8). Thus, further research is required to explore its clinical application.

DISCUSSION

Various compounds and peptides targeting the contact-kinin system have been developed, with the goal of combating cardiovascular diseases (CVD) such as IS, myocardial infarctions, and atherosclerosis through their anti-inflammatory and anti-thrombotic properties (Aygören-Pürsün et al., 2018, 2023; Banerji et al., 2017; Chen et al., 2019; Maetzel et al., 2022; Sheffer et al., 2011; Wilbs et al., 2020). Such research has highlighted the importance of targeting PK and/or FXIIa in treating cardiovascular disorders. However, these potential therapeutic agents face several challenges, including safety concerns, immunogenicity, off-targeting effects, and affordability. Bats are known for their remarkable longevity, lower tumor incidence, and ability to harbor viruses without developing clinical disease (Li et al., 2023a; Luo et al., 2021; Ulanovsky & Moss, 2007), suggesting significant medicinal potential. In this study, we identified a six-amino-acid sequence fragment, LE6, derived from the brain of the bat species *Myotis myotis*, which exhibited inhibitory activity against both PK and FXIIa. Our experiments provide preliminary evidence of the potential benefits of LE6 in the treatment of inflammation, thrombosis, and IS, with a low risk of bleeding.

Clot formation in blood vessels is primarily governed by coagulation, anticoagulation, and thrombolytic factors, with mutual stimulation between inflammation and thrombosis exacerbating the condition (Long et al., 2016; Yan et al., 2020a; Zhang et al., 2021). LE6 demonstrated potent inhibitory effects on thromboinflammation by targeting the contact system-activating factor FXIIa (Ki: 6.37 μmol/L), a critical factor in the coagulation cascade, and the kinin system-activating enzyme PK (Ki: 43.97 μmol/L), which reciprocally activates the inflammatory cascade in concert with FXIIa. The inhibition of FXIIa and PK effectively reduced thrombosis without compromising hemostasis. High activity levels of tPA, uPA, and plasmin are thrombolytic but also major contributors to bleeding (Dai et al., 2023; Verstraete &

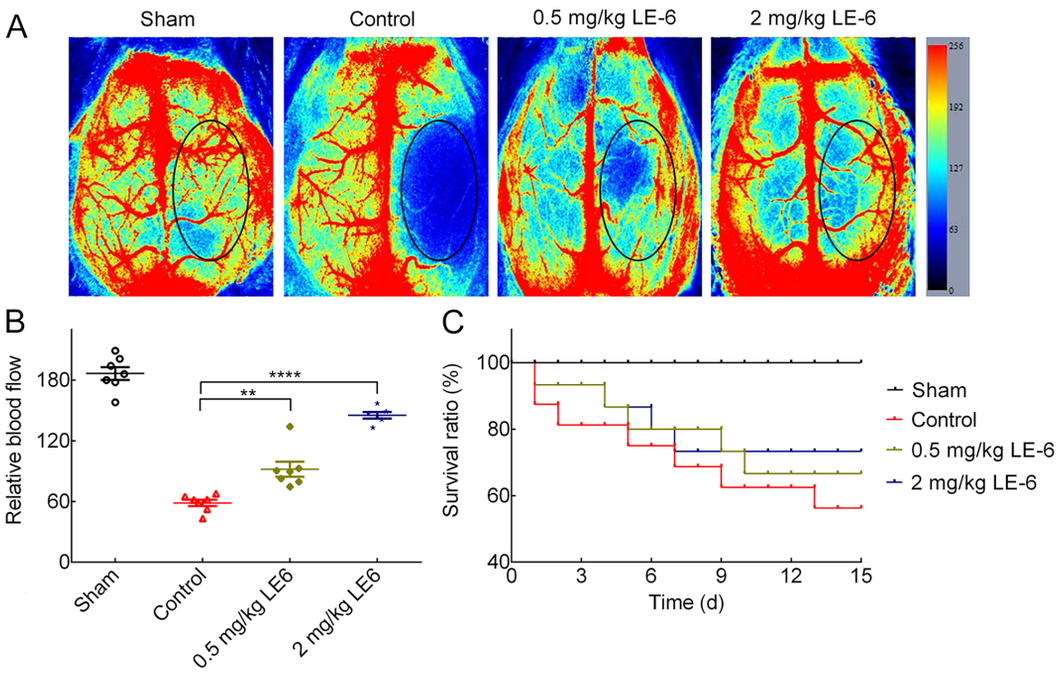

Figure 5 LE6 reduces photochemically induced cortical thrombosis

A–C: Male C57BL/6J mice (6 weeks old, *n*=6–7) were used to establish a cortical photothrombosis model after *i.v.* injection of 0.9% saline (control), heparin sodium (positive drug, 2 500 U/kg), or LE6 (0.5 or 2 mg/kg). Mice were subjected to LSP brain imaging one day after surgery (A), and blood flow of blood perfusion unit in the carotid artery ROI (black boxed area) was monitored by LSP imaging (B). Mouse survival was recorded over 15 consecutive days of LE6 administration (C). One-way ANOVA with Fisher's protected *t*-test was used in panel B. **: $P<0.01$; ****: $P<0.0001$. Data are presented as mean±SEM.

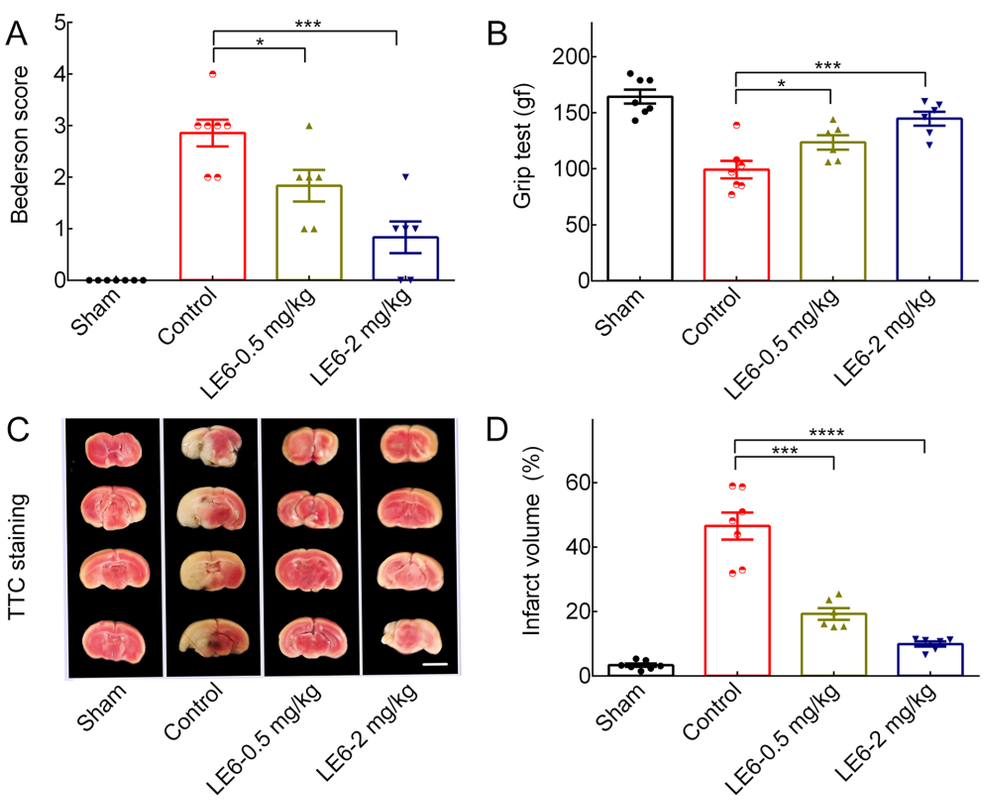

Figure 6 LE6 inhibits stroke injury in tMCAO mouse model

A–D: Male C57/6J mice (6 weeks old, *n*=6–8) underwent tMCAO surgery and were then *i.v.* injected with 0.9% saline (control) or LE6 (0.5 or 2 mg/kg) 15 min before reperfusion. After 24 h, mice were subjected to Bederson score analysis (A) and GST (B), then sacrificed. TTC-stained brain sections were imaged (C) (scale bar: 0.5 cm) for quantitative analysis (D). One-way ANOVA with Fisher's protected *t*-test was used in panels A, B, and D. *: $P<0.05$; ***: $P<0.001$; ****: $P<0.0001$. Data are presented as mean±SEM. tMCAO: Transient middle cerebral artery occlusion; TTC: 2,3,5-triphenyl tetrazolium chloride.

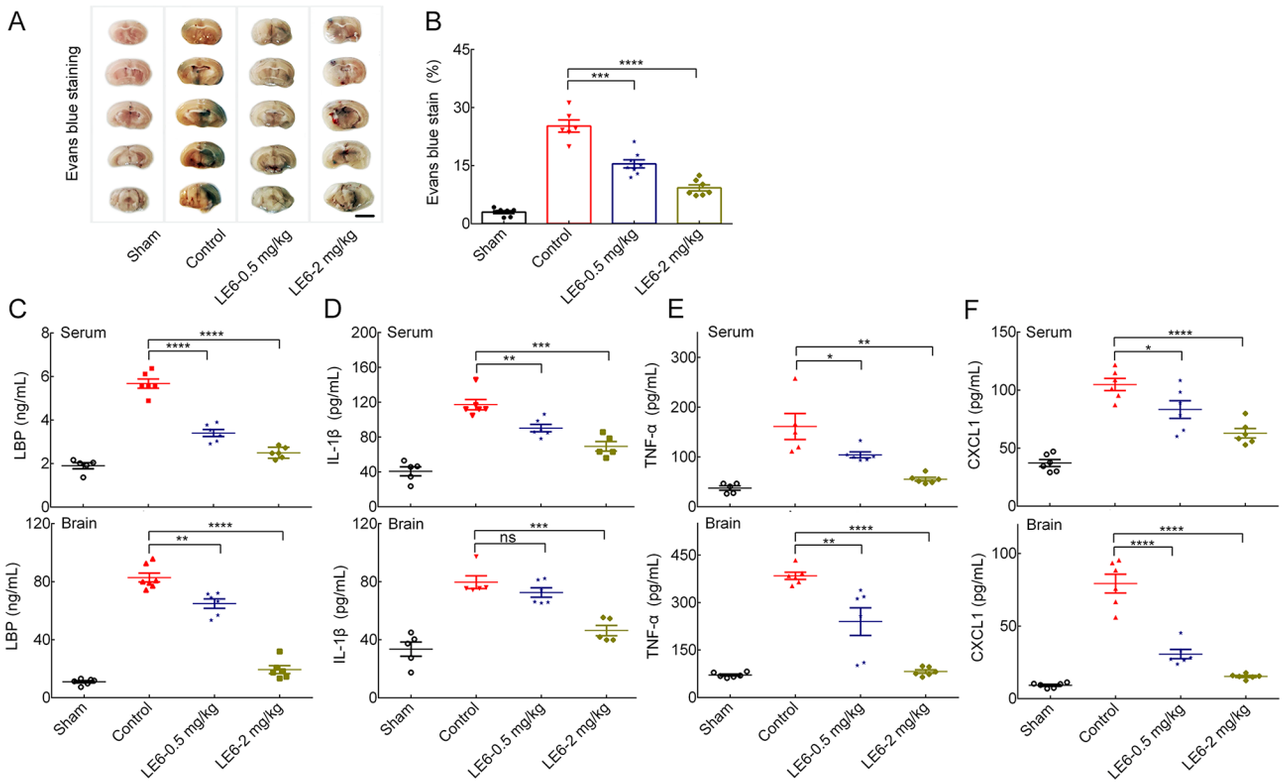

Figure 7 Effects of LE6 on BBB protection and inflammatory factor abatement in tMCAO model

A, B: Male C57BL/6J mice (6 weeks old, *n*=6–7) underwent tMCAO surgery and were then *i.v.* injected with different concentrations of LE6 and Evans blue stain solution before (15 min) and after reperfusion, respectively. After 24 h, brain tissues were sectioned for imaging (A) (scale bar: 0.5 cm) and Evans blue stained-sections were analyzed (B). C–F: ELISA analysis of LBP (C), IL-1β (D), TNF-α (E), and CXCL1 (F) concentrations in serum and brain homogenates of mice treated consistently in "Figures 7A, B" (24 h after tMCAO surgery). One-way ANOVA with Fisher's protected *t*-test was used in panel B-F. *: $P<0.05$; **: $P<0.01$; ***: $P<0.001$; ****: $P<0.0001$; ns: Not significant. Data are presented as mean±SEM.

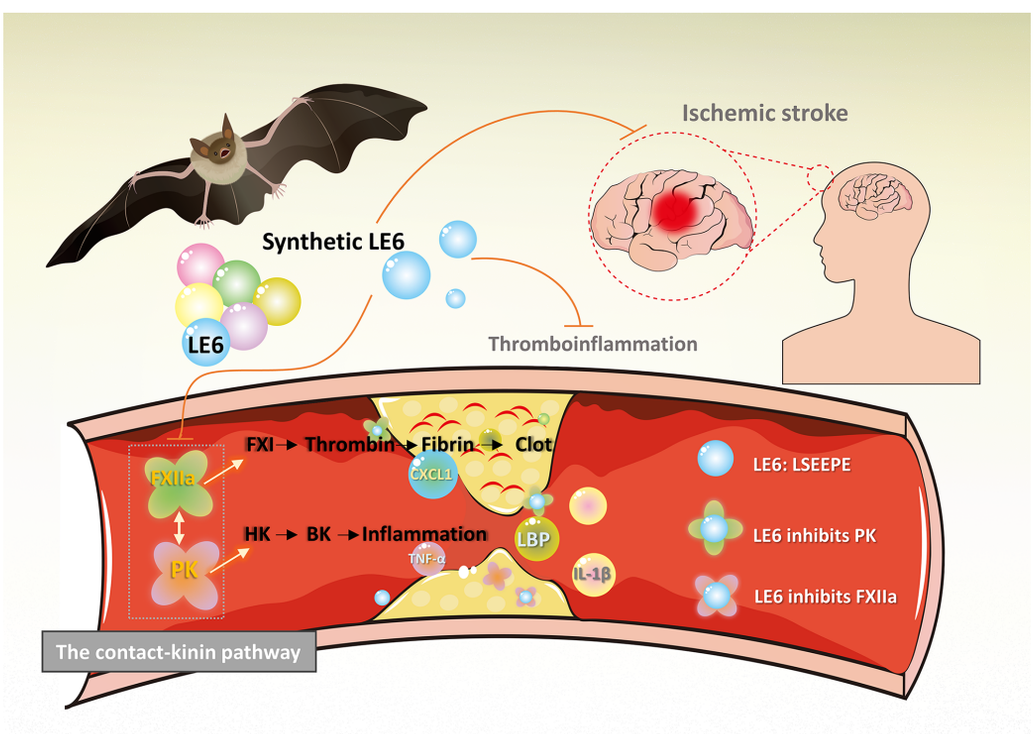

Figure 8 Bat-derived LE6 alleviates thromboinflammatory IS via inhibition of the contact kinin pathway

The contact-kinin pathway, involving PK and FXIIa, plays a crucial role in the pathogenesis of IS via inflammatory thrombosis. The oligopeptide fragment LE6, identified from the bat brain, exhibits therapeutic potential for thrombotic inflammatory and IS by inhibiting PK and FXIIa activity, with minimal hemorrhage risk.

Lijnen, 1994). While tPA is the only approved therapeutic agent for acute IS and is efficacious when administered within 4.5 hours of stroke onset, delayed administration can increase mortality in patients with intracranial hemorrhage (ICH), hemorrhagic transformation (HT), and IS (Kim, 2019; Simão et al., 2017). Hence, targeting the fibrinolytic systems during stroke intervention is not ideal. The suppression of tPA, uPA, and plasmin activity by LE6 may not necessarily be a disadvantage and may potentially offer yet to be identified benefits.

The interplay between thrombosis and inflammation significantly exacerbates the progression of IS. Our results demonstrated that LE6 effectively prevented intracranial thrombosis induced by photothrombosis, reducing intracranial stroke damage and improving survival in mice. Blood reperfusion following embolic recanalization can heighten the risk of inflammation and thrombus reformation in the brain. In this study, LE6 mitigated ischemia-reperfusion injury in tMCAO mice, as evidenced by reduced infarct size, lower inflammatory factor levels in the brain and periphery, and improved neurological function and BBB integrity.

Patients with CVD tend to experience higher rates of depression compared to the general population, with depression further exacerbating CVD conditions (Hare et al., 2014). Investigating the underlying pathogenic mechanisms linking depression and CVD is therefore crucial. Our previous research highlighted the significant role of immunoreactive LBP in regulating depression through the inhibition of monoamine synthesis (Fang et al., 2023b). As shown in Figure 7D, both brain and serum levels of LBP were increased in tMCAO mice but were reduced by *i.v.* administration of LE6. This elevation in LBP may be induced by inflammation (Fang et al., 2023b; Schumann et al., 1996). Therefore, by modulating FXIIa-PK activity, it may be possible to reduce LBP expression via decreased inflammation, potentially alleviating depression in patients with CVD. However, this hypothesis requires further exploration and validation through animal behavioral studies. Additionally, inflammation is implicated in the increased co-occurrence of CVD and depression among COVID-19 patients (Bucciarelli et al., 2022; Hare et al., 2014; Zheng et al., 2024). Thus, future inhibitors targeting FXIIa-PK, including LE6, hold promise for the treatment of these conditions.

In conclusion, this study demonstrated that the chemically synthesized oligopeptide LE6 effectively inhibited FXIIa and PK activity, providing robust anticoagulation in relevant animal disease models without increasing the risk of bleeding. This addresses several limitations associated with current heparin sodium therapy. The stability and cost-effectiveness of LE6 make it a suitable candidate for use in acute procedures or conditions with an elevated risk of thrombosis, such as vascular interventions in IS patients, without compromising hemostasis at the wound site.

COMPETING INTERESTS

The authors declare that they have no competing interests.

AUTHORS' CONTRIBUTIONS

M.Q.F., R.L., and L.N.C. designed the experiments. L.N.C. J.Y., and J.A.G. conducted most experiments, including enzyme activity analysis, SPR analysis, KLK-LE6 structure modeling, cellular experiments, animal experiments, and determination of related indicators. J.Y., X.L., X.L.C., R.C.T., Q.L., Q.M.L., and D.S.L. participated in the animal experiments and sample collection. M.Q.F., R.L., L.N.C., and J.Y. participated in data analysis and manuscript writing. M.Q.F. and R.L. conceived and supervised the project. All authors read and approved the final version of the manuscript.

ACKNOWLEDGMENTS

We would like to thank the Institutional Center for Shared Technologies and Facilities of Kunming Institute of Zoology (KIZ), Chinese Academy of Sciences (CAS) and Service Center for Bioactivity Screening, State Key Laboratory of Phytochemistry and Plant Resources, Kunming Institute of Botany, CAS, for providing Liquid Chromatography-Mass Spectrometry and SPR analysis. We are grateful to Lin Zeng and Lian Yang for their technical support.

REFERENCES

Aygören-Pürsün E, Bygum A, Grivcheva-Panovska V, et al. 2018. Oral plasma kallikrein inhibitor for prophylaxis in hereditary angioedema. *New England Journal of Medicine*, **379**(4): 352–362.

Aygören-Pürsün E, Magerl M, Graff J, et al. 2016. Prophylaxis of hereditary angioedema attacks: a randomized trial of oral plasma kallikrein inhibition with avoralstat. *Journal of Allergy and Clinical Immunology*, **138**(3): 934–936. e5.

Aygören-Pürsün E, Zanichelli A, Cohn DM, et al. 2023. An investigational oral plasma kallikrein inhibitor for on-demand treatment of hereditary angioedema: a two-part, randomised, double-blind, placebo-controlled, crossover phase 2 trial. *The Lancet*, **401**(10375): 458–469.

Banerji A, Busse P, Shennak M, et al. 2017. Inhibiting plasma kallikrein for hereditary angioedema prophylaxis. *New England Journal of Medicine*, **376**(8): 717–728.

Bird JE, Smith PL, Wang XK, et al. 2012. Effects of plasma kallikrein deficiency on haemostasis and thrombosis in mice: murine ortholog of the fletcher trait. *Thrombosis and Haemostasis*, **107**(6): 1141–1150.

Bucciarelli V, Nasi M, Bianco F, et al. 2022. Depression pandemic and cardiovascular risk in the COVID-19 era and long COVID syndrome: gender makes a difference. *Trends in Cardiovascular Medicine*, **32**(1): 12–17.

Chamorro Á, Dirnagl U, Urra X, et al. 2016. Neuroprotection in acute stroke: targeting excitotoxicity, oxidative and nitrosative stress, and inflammation. *The Lancet Neurology*, **15**(8): 869–881.

Chen ZL, Singh P, Wong J, et al. 2019. An antibody against HK blocks Alzheimer's disease peptide β-amyloid−induced bradykinin release in human plasma. *Proceedings of the National Academy of Sciences of the United States of America*, **116**(46): 22921–22923.

Dai W, Zhang H, Lund H, et al. 2023. Intracellular tPA–PAI-1 interaction determines VLDL assembly in hepatocytes. *Science*, **381**(6661): eadh5207.

Fang MQ, Cha JH, Wang HC, et al. 2023a. An undefined cystatin CsCPI1 from tea plant *Camellia sinensis* harbors antithrombotic activity. *Biomedicine & Pharmacotherapy*, **159**: 114285.

Fang MQ, Li Y, Liao ZY, et al. 2023b. Lipopolysaccharide-binding protein expression is increased by stress and inhibits monoamine synthesis to promote depressive symptoms. *Immunity*, **56**(3): 620–634. e11.

Franke M, Bieber M, Kraft P, et al. 2021. The NLRP3 inflammasome drives inflammation in ischemia/reperfusion injury after transient middle cerebral artery occlusion in mice. *Brain, Behavior, and Immunity*, **92**: 223–233.

Frazier AP, Mitchell DN, Given KS, et al. 2023. Chronic changes in oligodendrocyte sub-populations after middle cerebral artery occlusion in neonatal mice. *Glia*, **71**(6): 1429–1450.

GBD 2019 Stroke Collaborators. 2021. Global, regional, and national burden of stroke and its risk factors, 1990–2019: a systematic analysis for the Global Burden of Disease Study 2019. *The Lancet Neurology*, **20**(10): 795–820.

Girolami A, Candeo N, De Marinis GB, et al. 2011. Comparative incidence of thrombosis in reported cases of deficiencies of factors of the contact phase of blood coagulation. *Journal of Thrombosis and Thrombolysis*, **31**(1): 57–63.

Gao C, Xu Y, Liang Z, et al. 2021. A novel PGAM5 inhibitor LFHP-1c

protects blood-brain barrier integrity in ischemic stroke. *Acta Pharmaceutica Sinica B*, **11**(7): 1867–1884.

Göb E, Reymann S, Langhauser F, et al. 2015. Blocking of plasma kallikrein ameliorates stroke by reducing thromboinflammation. *Annals of Neurology*, **77**(5): 784–803.

Göbel K, Asaridou CM, Merker M, et al. 2019. Plasma kallikrein modulates immune cell trafficking during neuroinflammation via PAR2 and bradykinin release. *Proceedings of the National Academy of Sciences of the United States of America*, **116**(1): 271–276.

Hare DL, Toukhsati SR, Johansson P, et al. 2014. Depression and cardiovascular disease: a clinical review. *European Heart Journal*, **35**(21): 1365–1372.

Holland JM. 1976. Serotonin deficiency and prolonged bleeding in beige mice. *Experimental Biology and Medicine*, **151**(1): 32–39.

Ivanov I, Verhamme IM, Sun MF, et al. 2020. Protease activity in single-chain prekallikrein. *Blood*, **135**(8): 558–567.

Kale SS, Villequey C, Kong XD, et al. 2018. Cyclization of peptides with two chemical bridges affords large scaffold diversities. *Nature Chemistry*, **10**(7): 715–723.

Kearney KJ, Butler J, Posada OM, et al. 2021. Kallikrein directly interacts with and activates Factor IX, resulting in thrombin generation and fibrin formation independent of Factor XI. *Proceedings of the National Academy of Sciences of the United States of America*, **118**(3): e2014810118.

Kenne E, Renné T. 2014. Factor XII: a drug target for safe interference with thrombosis and inflammation. *Drug Discovery Today*, **19**(9): 1459–1464.

Kim JS. 2019. tPA Helpers in the treatment of acute ischemic stroke: are they ready for clinical use?. *Journal of Stroke*, **21**(2): 160–174.

Kleinschnitz C, Stoll G, Bendszus M, et al. 2006. Targeting coagulation factor XII provides protection from pathological thrombosis in cerebral ischemia without interfering with hemostasis. *The Journal of Experimental Medicine*, **203**(3): 513–518.

Lee JK, Park MS, Kim YS, et al. 2007. Photochemically induced cerebral ischemia in a mouse model. *Surgical Neurology*, **67**(6): 620–625.

Labat-gest V, Tomasi S. 2013. Photothrombotic ischemia: a minimally invasive and reproducible photochemical cortical lesion model for mouse stroke studies. *Journal of Visualized Experiments: JoVE*, **76**: 50370.

Li KQ, Liu GJ, Liu XY, et al. 2023a. EPAS1 prevents telomeric damage-induced senescence by enhancing transcription of *TRF1, TRF2*, and *RAD50. Zoological Research*, **44**(3): 636–649.

Li XJ, Qiao CC, Chen BJ, et al. 2022. Fuel source shift or cost reduction: Context-dependent adaptation strategies in closely related Neodon fuscus and Lasiopodomys brandtii against hypoxia. *Zoological Research*, **43**(4): 497–513.

Li YL, Jin T, Liu NX, et al. 2023b. A short peptide exerts neuroprotective effects on cerebral ischemia–reperfusion injury by reducing inflammation via the miR-6328/IKKβ/NF-κB axis. *Journal of Neuroinflammation*, **20**(1): 53.

Long AT, Kenne E, Jung R, et al. 2016. Contact system revisited: an interface between inflammation, coagulation, and innate immunity. *Journal of Thrombosis and Haemostasis*, **14**(3): 427–437.

Luo J, Liang S, Jin F. 2021. Gut microbiota in antiviral strategy from bats to humans: a missing link in COVID-19. *Science China Life Sciences*, **64**(6): 942–956.

Maetzel A, Smith MD, Duckworth EJ, et al. 2022. KVD900, an oral on-demand treatment for hereditary angioedema: phase 1 study results. *Journal of Allergy and Clinical Immunology*, **149**(6): 2034–2042.

Nitzsche A, Poittevin M, Benarab A, et al. 2021. Endothelial $S1P_1$ signaling counteracts infarct expansion in ischemic stroke. *Circulation Research*, **128**(3): 363–382.

Renné T. 2015. The vascular side of plasma kallikrein. *Blood*, **125**(4): 589–590.

Renné T, Pozgajová M, Grüner S, et al. 2005. Defective thrombus formation in mice lacking coagulation factor XII. *The Journal of Experimental Medicine*, **202**(2): 271–281.

Revenko AS, Gao DC, Crosby JR, et al. 2011. Selective depletion of plasma prekallikrein or coagulation factor XII inhibits thrombosis in mice without increased risk of bleeding. *Blood*, **118**(19): 5302–5311.

Sala-Cunill A, Björkqvist J, Senter R, et al. 2015. Plasma contact system activation drives anaphylaxis in severe mast cell–mediated allergic reactions. *Journal of Allergy and Clinical Immunology*, **135**(4): 1031–1043. e6.

Schumann RR, Kirschning CJ, Unbehaun A, et al. 1996. The lipopolysaccharide-binding protein is a secretory class 1 acute-phase protein whose gene is transcriptionally activated by APRF/STAT-3 and other cytokine-inducible nuclear proteins. *Molecular and Cellular Biology*, **16**(7): 3490–3503.

Sheffer AL, Campion M, Levy RJ, et al. 2011. Ecallantide (DX-88) for acute hereditary angioedema attacks: integrated analysis of 2 double-blind, phase 3 studies. *Journal of Allergy and Clinical Immunology*, **128**(1): 153–159. e4.

Shuaib A, Butcher K, Mohammad AA, et al. 2011. Collateral blood vessels in acute ischaemic stroke: a potential therapeutic target. *The Lancet Neurology*, **10**(10): 909–921.

Simão F, Ustunkaya T, Clermont AC, et al. 2017. Plasma kallikrein mediates brain hemorrhage and edema caused by tissue plasminogen activator therapy in mice after stroke. *Blood*, **129**(16): 2280–2290.

Tang XP, Fang MQ, Cheng RM, et al. 2020. Iron-deficiency and estrogen are associated with ischemic stroke by up-regulating transferrin to induce hypercoagulability. *Circulation Research*, **127**(5): 651–663.

Ulanovsky N, Moss CF. 2007. Hippocampal cellular and network activity in freely moving echolocating bats. *Nature Neuroscience*, **10**(2): 224–233.

Verstraete M, Lijnen HR. 1994. Novel thrombolytic agents. *Cardiovascular Drugs and Therapy*, **8**(6): 801–811.

Wei XH, Zhang BP, Wei FY, et al. 2022. Gegen Qinlian pills alleviate carrageenan-induced thrombosis in mice model by regulating the HMGB1/NF-κB/NLRP3 signaling. *Phytomedicine*, **100**: 154083.

Wilbs J, Kong XD, Middendorp SJ, et al. 2020. Cyclic peptide FXII inhibitor provides safe anticoagulation in a thrombosis model and in artificial lungs. *Nature Communications*, **11**(1): 3890.

Yan CC, Zhang XS, Zhou L, et al. 2020a. Effects of aging on gene expression in blood of captive Tibetan macaques (*Macaca thibetana*) and comparisons with expression in humans. *Zoological Research*, **41**(5): 557–563.

Yan HF, Tuo QZ, Yin QZ, et al. 2020b. The pathological role of ferroptosis in ischemia/reperfusion-related injury. *Zoological Research*, **41**(3): 220–230.

Yin SG, Pang AL, Liu CX, et al. 2022. Peptide OM-LV20 protects astrocytes against oxidative stress *via* the 'PAC1R/JNK/TPH1' axis. *Journal of Biological Chemistry*, **298**(10): 102429.

Zamolodchikov D, Chen ZL, Conti BA, et al. 2015. Activation of the factor XII-driven contact system in Alzheimer's disease patient and mouse model plasma. *Proceedings of the National Academy of Sciences of the United States of America*, **112**(13): 4068–4073.

Zamolodchikov D, Renné T, Strickland S. 2016. The Alzheimer's disease peptide β-amyloid promotes thrombin generation through activation of coagulation factor XII. *Journal of Thrombosis and Haemostasis*, **14**(5): 995–1007.

Zhang P, Chen JS, Li QY, et al. 2021. Neuroprotectants attenuate hypobaric hypoxia-induced brain injuries in cynomolgus monkeys. *Zoological Research*, **41**(1): 3–19.

Zhang ZY, Shen CB, Fang MQ, et al. 2022. Novel contact–kinin inhibitor sylvestin targets thromboinflammation and ameliorates ischemic stroke. *Cellular and Molecular Life Sciences*, **79**(5): 240.

Zheng HY, Song TZ, Zheng YT. 2024. Immunobiology of COVID-19: Mechanistic and therapeutic insights from animal models. *Zoological Research*, **45**(4): 747–766.

Zuraw B, Yasothan U, Kirkpatrick P. 2010. Ecallantide. *Nature Reviews Drug Discovery*, **9**(3): 189–190.